Applied Clay Science 182 (2019) 105284

Contents lists available at ScienceDirect

Applied Clay Science

journal homepage: www.elsevier.com/locate/clay

Research Paper

Unidirectional kaolinite dissolution rates at near-equilibrium and near-neutral pH conditions

Lei Gong[a], J. Donald Rimstidt[b,1], Yilun Zhang[a], Kaiyun Chen[c], Chen Zhu[a,*]

[a] Department of Earth and Atmospheric Sciences, Indiana University, Bloomington, IN 47405, USA
[b] Department of Geosciences, Virginia Tech, Blacksburg, VA 24061, USA
[c] Northwest University, Department of Geology, State Key Laboratory Continental Dynamics, Xi'an 710069, China

ARTICLE INFO

Keywords:
Kinetics
Si isotopes
Kaolinite
Clay
MC-ICP-MS
Non-traditional isotopes

ABSTRACT

Kaolinite dissolution rates at ambient temperature and pH 7.1–8.5 were measured with the isotope tracer method. A rare Si isotope ^{29}Si was introduced to the experimental solutions, which reacted with Georgia kaolinite (KGa-1b) composed of mostly ^{28}Si. Reaction rates were tracked by $^{29}Si/^{28}Si$ ratios of reacted solutions. The 16 batch experiments were designed with a grid of solutions that ranged from near saturation to supersaturation with respect to kaolinite. An average dissolution rate (unidirectional) of $5.4 \pm 1.6 \times 10^{-14}$ mol (kaol) s^{-1} m^{-2} consistently fitted the $^{29}Si/^{28}Si$ ratios for all 16 experiments, indicating the dissolution rates were independent of pH in near-neutral pH waters and independent from the levels of departure from equilibrium. In other words, it appears that the dissolution reaction mechanisms do not change across from the kaolinite-undersaturated to kaolinite-supersaturated solutions near-equilibrium.

The near-equilibrium kaolinite dissolution rates in this study are a new type of rates—unidirectional rates (from the isotope tracer method), which differ from all near-equilibrium kaolinite dissolution rates in the literature that are based upon Si or Al concentrations and are net rates (dissolution minus precipitation rates). Kaolinite dissolution was non-stoichiometric in all experiments. The Si and Al concentrations were sometimes systematic but more often erratic, resulting from the precipitation of Al–Si secondary phases. The experimental solutions were grossly supersaturated with respect to gibbsite, allophanes, and imogolites. This confirms our hypothesis that the scatter and conflicts of near-equilibrium data are caused by unaccounted-for secondary phase precipitation, but the isotope tracer method successfully circumvents this experimental pitfall. Most natural waters are supersaturated with clays and are near-neutral pH. Our experimental rates are more applicable to the studies of natural waters than the majority rates available in the literature, which have mostly been measured at far-from-equilibrium, acidic pH, and high temperatures.

1. Introduction

The kinetics of clay mineral reactions, namely the rates and mechanisms of dissolution and precipitation, is significant to a number of geological and environmental processes. For example, some proposed geological repositories of high-level nuclear wastes are within thick shale formations (Madsen, 1998). The production of natural gas from shale also involves reactions of fluids with clays. Most natural waters at ambient temperature are either near-equilibrium or supersaturated with respect to clays (Drever, 1988; Langmuir, 1997; McBride, 1994). Therefore, kinetics data for clay minerals at near-equilibrium are needed.

However, near-equilibrium kinetics data for clays are scarce. For kaolinite—arguably the most important clay mineral for both a model clay mineral and industrial applications (Murray, 1999)—three experiments have been conducted (Devidal et al., 1997; Nagy et al., 1991; Yang and Steefel, 2008), which is more than for any other clays. These experiments were conducted at high temperature or at either alkaline or acidic pH, and the resulting rate data do not agree with each other.

This paucity of rate data under near-equilibrium conditions for clays is mostly due to the limits of the *conventional experimental method*, which relies upon Si or Al concentration to derive dissolution and precipitation rates. This method is unworkable in the presence of secondary phase precipitation. While this situation is true for most silicate minerals, the challenge is exacerbated for clay minerals because they have low solubility and are among the slowest reacting silicate

* Corresponding author.
E-mail address: chenzhu@indiana.edu (C. Zhu).
[1] Author passed away.

https://doi.org/10.1016/j.clay.2019.105284
Received 13 June 2019; Received in revised form 26 August 2019; Accepted 27 August 2019

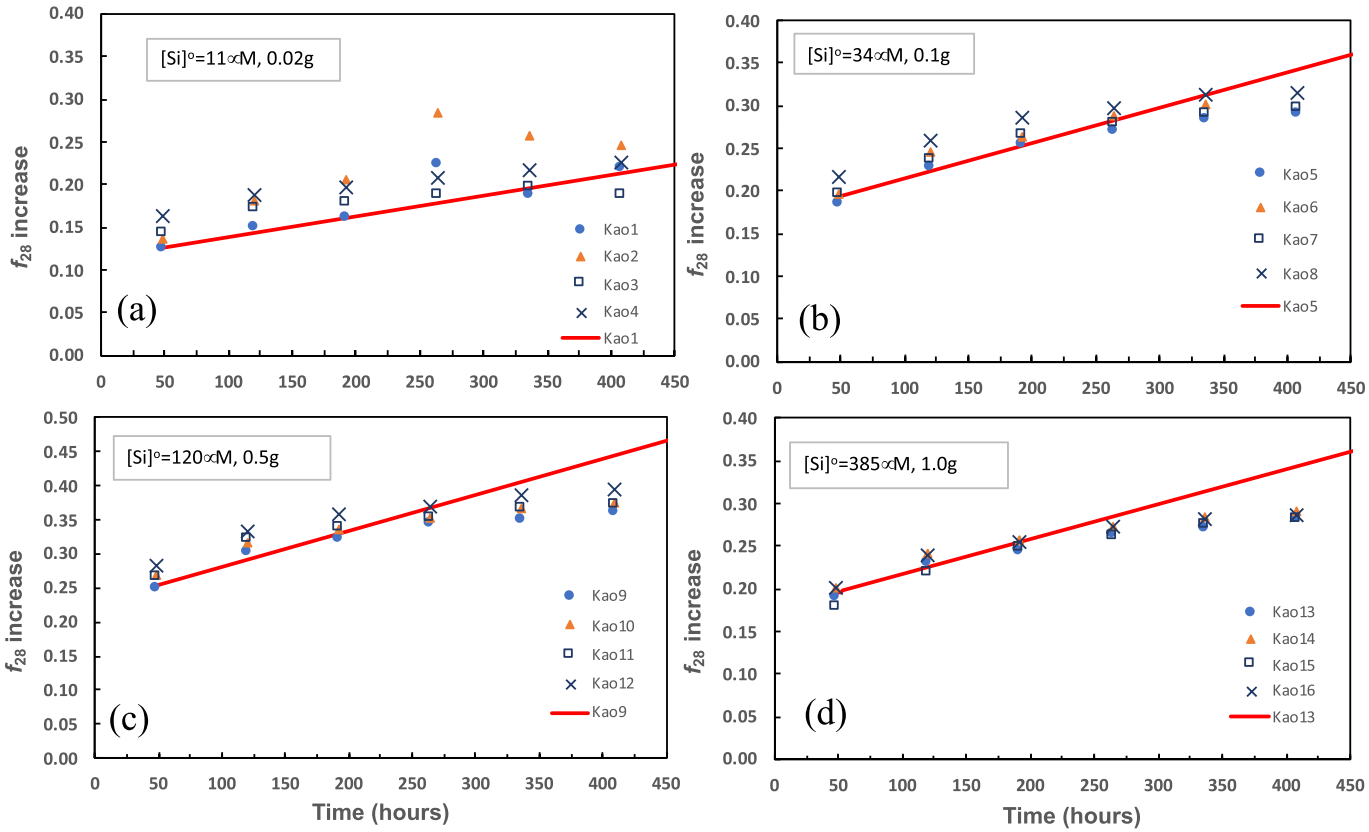

Fig. 1. Increase of Si isotope fractional abundances in experimental solution from the initial solutions. Symbols represent experimental data. Analytical uncertainties for isotope fraction (f_{28}) are smaller than the symbols (< ± 0.01, 2σ). The lines were fitted with Eq. (1). For the clarity, only one line is shown for each group. The f_{28} values and temporal evolution varies from batch to batch, as they should, because they change with solid:solution ratios and initial Si concentrations ([Si]°).

minerals. For example, the kaolinite rates are two orders of magnitude slower than feldspar rates (Brantley, 2008).

Near-equilibrium conditions also result in a high level of Si and Al concentrations in the solutions, leading to supersaturation with a number of Al- and Si-bearing amorphous or poorly crystalline phases that precipitate. Therefore, most near-equilibrium kaolinite kinetics experiments have historically been performed in the acidic (e.g., pH 2–4) or alkaline pH. At near-neutral pH conditions under which clay solubilities are lowest, the experimental data even at far-from-equilibrium conditions are scattered and inconsistent (e.g., Fig. 1 of the middle panel of Huertas et al., 1999; and detailed discussions in Yang and Steefel, 2008).

Recently, Zhu and collaborators used an innovative ^{29}Si isotope tracer method to study quartz and albite reaction rates (Gruber et al., 2013; Liu et al., 2016; Zhu et al., 2016), achieving orders-of-magnitude improvements in detection sensitivity and with promises to overcome the longtime experimental barriers to measuring slow near-equilibrium reaction rates. Because the rates are based on isotope ratios instead of Si or Al concentration, the method works in the presence of secondary phase precipitates. The controversy over stoichiometric versus non-stoichiometric dissolution (i.e., whether [Si]:[Al] = 2:2 for kaolinite; See Table 1 for symbols and definitions) becomes irrelevant.

Here, we present a batch experimental study to test the hypothesis that the scatter and conflicts of near-equilibrium data are caused by unaccounted-for secondary phase precipitation, and that the isotope tracer method circumvents this experimental pitfall. Sixteen batch experiments were carried out following a grid of pH and [Si] to examine the dissolution rate dependence on pH and kaolinite saturation. The experimental data generated kaolinite dissolution rates that are appropriate for applications to natural systems. We will also discuss the implications for future clay kinetics studies.

Table 1
List of symbols and definitions.

Symbols	Definitions
f_{28}	^{28}Si fractional abundance (0 to 1) in experimental solution $f_{28} = {}^{28}Si/\{{}^{28}Si + {}^{29}Si + {}^{30}Si\}$; $f_{28} = \frac{1}{1+R_{29/28}+R_{30/28}}$where $R_{29/28} = {}^{29}Si/{}^{28}Si$ denotes the ratios of isotope abundnance; similarly for f_{29} and f_{30}.
$\Delta_f G^o$	The standard Gibbs free energy of formation (kJ mol^{-1})
$\Delta_r G^o$	Gibbs free energy of reaction (e.g., kaolinite dissolution) (kJ mol^{-1})
K	Equilibrium constant
K_{sp}	Solubility products
r_+	Forward rate of kaolinite dissolution in mol (kaol) m^{-2} s^{-1}
$r'_{+,Si}$	Forward rate of kaolinite dissolution in mol (Si) L^{-1} s^{-1}; $r'_{+,Si} = 2 \times r'_{+,kaol}$
r'_+	Forward rate of kaolinite dissolution in mol (kaol) L^{-1} s^{-1}; $r'_+ = r_+ S_A$
$r'_{pre,Si}$	The total Si precipitation rate in mol (Si) L^{-1} s^{-1}
$r'_{pre,Al}$	The total Al precipitation rate mol (Al) L^{-1} s^{-1}
S_A	Surface area load of kaolinite (m^2/L) in the reactor;
[Si]	Total concentration of element or species of Si (mol L^{-1}); similar for Al; Superscripts denote time
Abbrev	
am	Amorphous
aq	Aqueous species
kaol	Kaolinite
pre	Precipitation
SI	Saturation index SI = log(Q/K) = $RT\,\Delta_r G$, where R is the gas constant and T the temperature (K)

2. Materials and methods

In this study, all experiments were carried out at Indiana University. Experiments were conducted at temperature of ~22 ± 0.5 °C.

2.1. Kaolinite sample preparation

Low defect Georgia kaolinite, KGa-1b, was purchased from the Clay Minerals Society. This kaolinite has been extensively characterized (e.g., Thompson, 1998). In brief, KGa-1b consists of euhedral hexagonal kaolinite platelets (0.1 to 15 μm diameter) and larger (up to 25 μm) vermicular stacks of kaolinite platelets. It has an N_2-BET specific surface area of 11.38 $m^2\,g^{-1}$; individual kaolinite crystals are chemically pure and stoichiometric and they are highly crystalline (Thompson et al., 1999).

Samples pre-treatment followed the procedures of Yang and Steefel (2008). Samples were cleaned prior to dissolution and precipitation experiments to remove amorphous oxy-hydroxide material by washing with 1 M NaCl/HCl at pH 3 until the supernatant pH reached 3, followed by repeatedly rinsing with ultra-pure H_2O (18.3 MΩ·cm) and vacuum filtration through 0.22 μm polyethersulfone (PES) membrane filter until pH > 5. The cleaned and rinsed samples were then dried at 50 °C in the oven, gently crushed and stored in a HDPE bottle. In general, the natural abundances of Si isotopes vary insignificantly for the purpose of isotope tracer kinetics studies. They are assumed to have the abundances of 0.9223, 0.0467, and 0.0310 for ^{28}Si, ^{29}Si, and ^{30}Si, respectively (Opfergelt and Delmelle, 2012).

2.2. ^{29}Si stock solution for isotope tracer experiments

Except where noted, all chemicals used were analytical grade. In order to prepare the ^{29}Si stock solution, $^{29}SiO_2$ enriched powder (with isotope fractional abundance of 0.0004 ^{28}Si, 0.9990 ^{29}Si, and 0.0006 ^{30}Si from Isoflex, San Francisco, CA, USA) were dissolved by alkali flux. Briefly, 0.0488 (± 0.001) g of $^{29}SiO_2$ powder and 0.3200 (± 0.001) g of NaOH were placed in a silver crucible that was subsequently put into a 730 °C preheated muffle furnace and held for 10 min. After cooling to room temperature, the mixture was dissolved in 500 mL DI water and was vacuum-filtered (Thermo Scientific, Nalgene, sterile analytical filter). The solution was then transferred into a clean 500-mL polypropylene bottle. To remove Na^+, the diluted solution (1.6 mM $^{29}SiO_2$) was passed through multiple columns filled with Bio-Rad cation exchange resin AG-50 W-X8 (100 to 200 mesh) in H^+ form. The ion-exchanged solution was collected into a new, clean polypropylene bottle and stored at 4.0 °C.

2.3. Dissolution experiments with isotope doping at different pH and saturation state

The initial solution was prepared by mixing a certain amount of $AlCl_3{\cdot}6H_2O$, and KH_2PO_4-Na_2HPO_4 (for pH 7.0–7.5) or H_3BO_3-NaB$(OH)_4$ (for pH 8.0–8.5) pH buffer solution, DI water, and $^{29}SiO_2$ stock solution, with a final volume of 250 mL. The pH of the initial solution was thereafter measured and adjusted by adding a small amount of HCl or NaOH to achieve the desired pH values. A pre-selected mass of kaolinite (see Table 2) and 20 mL initial solution with different pH and Si concentrations were mixed in a 30-mL polypropylene bottle to initiate mineral dissolution. Overall, several polypropylene bottles were prepared for each group of batch experiments. One sample, with no kaolinite added, was used as the experimental control. The bottles were agitated on an orbital shaker at ~100 rpm. The experimental grid is shown in Table 2.

The above grid gave us 16 rate data points from 16 batch experiments. For each batch experiment, we had six samples time series data points, sampled from 48 to 408 h after the reactions.

2.4. Sampling of dissolution experiments

At pre-determined sampling intervals, the bottles were taken down. The solids and solutions were separated by centrifugation at a maximum relative centrifugal force of 4700 (RCF, g-force) for 20 min and the liquid supernatant was collected and filtered. The solution was first filtered with a 0.22 μm Nylon membrane syringe filter, and then filtered again with 0.1 μm Nylon syringe filter (Sterlitech Corporation, Kent, WA USA) to remove small kaolinite particles. The filtered solution was divided into four fractions (~3 mL each) for ICP-OES analysis of Si and Al concentrations, Si isotope analysis with ICP-QMS, pH analysis, and reserve. The pH of the solution was measured at room temperature 22.5 (± 0.5) °C determined immediately after sample collection using an Orion™ 8102BNUWP ROSS Ultra™ pH Electrode. The reported accuracy was ± 0.02 pH units (i.e. ± 4.5% in H^+ activity).

2.5. ICP-QMS measurements

ICP-MS analysis of Si isotope ratios was conducted with an Agilent 7700 at Indiana University. The sample uptake rate is 0.3 mL/min. Between each analysis, the system was rinsed with 2% HNO_3 for 30 s and then washed with Milli-Q water twice for 60 s each time.

For each sample measured on the ICP-QMS instrument, three m/z channels were measured for ^{28}Si, ^{29}Si, and ^{30}Si, respectively. Ten replicate analyses were performed for the analysis of each channel, and each analysis consisted of 100 sweeps, each with an integration time of 0.1 s. The signal intensity of CPS value and the associated RSD based on the ten replicate analysis was reported for each m/z channel. For ^{28}Si and ^{29}Si measurements, the RSDs of the QMS measurements in this study are generally below 3% for the samples with ~250 ng/mL of total Si concentration. For ^{30}Si measurements, due to its low concentration and large interferences from the polyatomic species, the signal to noise ratio is too low, and thus not used in this study.

2.5.1. Determination of Si and cation concentrations

Total dissolved Si and Al concentrations (i.e., [Si]) were analyzed with Thermo-Scientific iCAP 7400 ICP-OES. The uncertainty in measured Si was less than < ± 4% (RSD) for concentrations above 4 μM. Detection limits for analyses of Si were < 50 ppb (or 2 μM) and of Al < 10 ppb (or 0.33 μM).

2.5.2. Calculations of mineral saturation indices and reaction rates

Based on the measured concentrations of Si, Al, and pH (all data can be found in electronic supplementary material), saturation indices (SI) for kaolinite were calculated with the aid of the software PHREEQC 3.5.0 (Parkhurst and Appelo, 2013). An internally consistent dataset of equilibrium constants for relevant mineral and aqueous species at 50 °C was constructed using SUPCRTBL (Zimmer et al., 2016). For amorphous SiO_2 and $Al(OH)_3$, log*K*s were taken from Stefansson (2001). For allophane and imogolite, thermodynamic properties were re-calculated based on the experimental data in Su and Harsh (1994, 1998). The Gibbs free energy at standard state for those species was adjusted to ensure the internal consistency with other species in Zimmer et al. (2016).

As shown by Zhu et al. (2016), for a batch reactor system, considering both primary mineral dissolution and secondary phase precipitation, the temporal evolution of silica concentration and silicon isotope composition can be described with a set of mass balance equations (isotope fractionation due to both dissolution and precipitation can be neglected):

$$[\mathrm{Si}]^{t+1} = (2r'_{+} - r'_{pre,\mathrm{Si}})\Delta t + [\mathrm{Si}]^{t} \quad (1)$$

$$[^{28}\mathrm{Si}]^{t+1} = (2f_{28,\mathrm{kaol}}\, r'_{+} - f_{28,t}\, r'_{pre,\mathrm{Si}})\Delta t + f_{28,t}\,[\mathrm{Si}]^{t} \quad (2)$$

$$[^{29}\mathrm{Si}]^{t+1} = (2f_{28,\mathrm{kaol}}\, r'_{+} - f_{29,t}\, r'_{pre,\mathrm{Si}})\Delta t + f_{29,t}\,[\mathrm{Si}]^{t} \quad (3)$$

For constant dissolution and precipitation rates, Eqs. (1–3) are solvable analytically,

Table 2
The experimental matrix and results.

Expt	Solids	pH	pH	Si[c]	[a]$r_{+,\text{kaol}}\times10^{14}$	$r'_{+,\text{Si}}\times10^{11}$	$r'_{prep,\text{Si}}\times10^{11}$	$r'_{prep,\text{Al}}\times10^{11}$	SI (kaol)
#	(g)	Initial	Final	(μM)	mol m^{-2} s^{-1}	mol L^{-1} s^{-1}	mol L^{-1} s^{-1}	mol L^{-1} s^{-1}	
Kao1	0.02	7.18	7.16	10	5.10	0.12	0	us[b]	4.72
Kao2	0.02	7.61	7.58	10	9.65	0.28	0	us[b]	3.52
Kao3	0.02	7.84	7.77	10	4.78	0.13	0,us[b]	us[b]	1.38
Kao4	0.02	8.44	8.29	10	5.18	0.12	0, us[b]	us[b]	1.26
Kao5	0.1	7.17	7.16	30	6.90	0.81	0	us[b]	5.05
Kao6	0.1	7.66	7.59	30	6.41	0.76	0	us[b]	4.7
Kao7	0.1	8.04	7.78	30	6.45	0.76	0.56	0.67	2.16
Kao8	0.1	8.50	8.32	30	6.76	0.80	0.56	0.68	2.07
Kao9	0.5	7.19	7.16	100	5.43	3.20	3.16	3.27	6.13
Kao10	0.5	7.64	7.58	100	4.64	2.74	2.34	3.27	3.25
Kao11	0.5	7.93	7.67	100	4.22	2.49	2.00	3.35	3.27
Kao12	0.5	8.51	8.29	100	4.05	2.39	2.51	3.35	2.64
Kao13	1	7.19	7.13	300	4.76	5.62	7.94	6.61	6.65
Kao14	1	7.63	7.51	300	4.14	4.88	7.94	6.61	6.35
Kao15	1	8.02	7.51	300	4.17	4.92	6.46	6.62	5.35
Kao16	1	8.62	8.26	300	2.74	3.20	5.01	6.68	3.75

[a] When comparing rates, kaolinite dissolution rate has a stoichiometric coefficient of 2 for Si and Al; the precipitation rate of Si and Al has a stoichiometric coefficient of 1. For easy comparison, kaolinite dissolution rates were also calculated as Si flux $r_{+,\text{Si}}$ in mol L^{-1} s^{-1}.
[b] Us: unsystematic concentration evolution with time. If a number precedes, it means [Al] or [Si] initially had a pattern and then became unsystematic.
[c] Target concentration. Actual initial concentration varied. Target [Al] was 0.3 μM but actual initial [Al] varied from 1.02 to 2.37 μM.

$$\begin{cases} f_{28,t} = f_{28,kaol} - (f_{28,kaol} - f_{28,t0})\left(\dfrac{2r'_{+} - r'_{pre,Si}}{[\text{Si}]^{t0}}t + 1\right)^{\frac{-2r'_{+}}{2r'_{+}-r'_{pre,Si}}} \\ f_{29,t} = f_{29,kaol} - (f_{29,kaol} - f_{29,t0})\left(\dfrac{2r'_{+} - r'_{pre,Si}}{[\text{Si}]^{t0}}t + 1\right)^{\frac{-2r'_{+}}{2r'_{+}-r'_{pre,Si}}} \end{cases} \quad (4)$$

With the aid of Excel® solver, steady-state rates can be fitted to experimental data of $f_{28,t}$ and $f_{29,t}$. In practice, $f_{28,t}$ and $f_{29,t}$ are not sensitive to $r'_{\text{pre,Si}}$ unless the percentage of Si precipitated is large relative to the solution [Si]. This means that the dissolution rate r_+ can be measured while Si precipitation occurs (Zhu et al., 2016). However, the method cannot distinguish between the reverse reaction of kaolinite dissolution (kaolinite precipitation) and precipitation of a Si-containing secondary phase such as allophane. Consequently, $r'_{pre,\text{ Si}}$ stands for the rate of removal of silica from solution (mol L^{-1} s^{-1}) as a combined result of all Si precipitation reactions that occur in the system.

3. Results

The temporal evolution of Si isotope fractional abundances (f_{28}) is shown in Fig. 1. The majority of the data are consistent and systematic, with the exception of three outliers (Kao2–4, 2–5 and Kao6–6, the second digit in sample # denotes the *n*th sample in the batch). In all experiments, f_{28} values increased and the ^{29}Si fraction (f_{29}) decreased monotonically, forming smooth, temporal evolution trends. These trends allowed the use of Eq. (4) to calculate kaolinite dissolution rates, r_+ (mol m^{-2} s^{-1}). The best r_+ values for each experiment were found with Excel® solver with the objective function to minimize the differences between experimental f_{28} or f_{29} data and model fittings. The rates were normalized with BET surface area for inter-experiment comparison. In experiments with high solid:solution ratios (Kao9–12 and Kao13–16, Fig. 2c,d), there was a deceleration of the f_{28} increase with time—the curves become flattened. The first four data points were used for rate retrieval according to the initial rate method for batch reactors (Rimstidt, 2014). The derived rates are close to each other (Table 2) and the average value is $5.4 \pm 1.6 \times 10^{-14}$ mol m^{-2} s^{-1}.

Note that the rates show no dependence on saturation levels, pH, or solid:solution ratios. See more discussion below on saturation levels with respect to kaolinite. Eight experiments used KH_2PO_3-Na_2HPO_4 as the pH buffer; the other eight used H_3BO_3-$NaB(OH)_4$ as the pH buffer. No differences in rates from experiments with the two buffers could be discerned.

During the experiments, the solution pH was stable for the batches at pH ~7.16 and ~7.62. The solutions intended for pH 8.5 drifted to ~8.3. The solutions intended to be pH 8.0 drifted to about 7.7. See Table 2 for the pH values in the initial and final solutions. The dissolution of kaolinite at pH 7.1–8.5 produces hydronium into the solutions through the reaction:

$$Al_2Si_2O_5(OH)_4 + 7\ H_2O \rightarrow 2\ Al(OH)_4^- + 2H_4SiO_{4(aq)}^o + 2\ H^+ \quad (R1)$$

Nearly all experimental solutions were grossly supersaturated with respect to gibbsite, imogolites, and allophanes, some supersaturated with respect to quartz, but all undersaturated with respect to amorphous $Al(OH)_3$ and amorphous silica. The degree of saturation with respect to the Al—Si phases (kaolinite, allophanes, and imogolites) was a function of pH and [Si] level. The solubilities of these phases have a minimum near pH 6–6.5. From pH 7.16 to 8.5, their solubilities increase about an order of magnitude.

The [Si] data for the experiments are shown in Fig. 2, and the [Al] data are available in the electronic supplement. Note that [Al] was under the detection limit for many samples and the low concentration data carry large uncertainties. The [Si] and [Al] data show that kaolinite dissolution was non-stoichiometric with dissolved [Si] > [Al], indicating more and faster precipitation of Al than Si. In the pH 7.16 and 7.62 solutions with initial [Si] of 10 and 30 μM (Kao1, Kao2, Kao5, Kao6), the Si concentrations increased monotonically at the same rate as indicated by the isotope ratios. However, in all pH ~8.0 and ~8.5 and [Si] 100 and 300 μM solutions, Si increased at rates much slower than kaolinite dissolution rates, indicating precipitation of Si-containing secondary phases. In the group of experiments with an initial [Si] of 300 μM, net Si precipitation occurred, resulting in a decrease of [Si] over time (Fig. 2d).

The initial $[\text{Si}]^o$ and Si dissolved from kaolinite ($\Delta[\text{Si}]_{\text{kaol}}$) minus the experimentally observed $[\text{Si}]^t$ represent the amounts of Si that were precipitated from the solutions (see the mass balance in Eq. 1). The red solid lines in Fig. 2 stand for the ($[\text{Si}]^o + \Delta[\text{Si}]_{\text{kaol}}$) values and the blue lines were fitted to the experimental [Si] with Si precipitation rates. See Table 2 for rates for each experiment. Apart from experiments with pH 7.16 and 7.62 and [Si] of 10 and 30 μM (Kao1, Kao2, Kao5, Kao6), all experiments precipitated significant amounts of Si-containing phase (s).

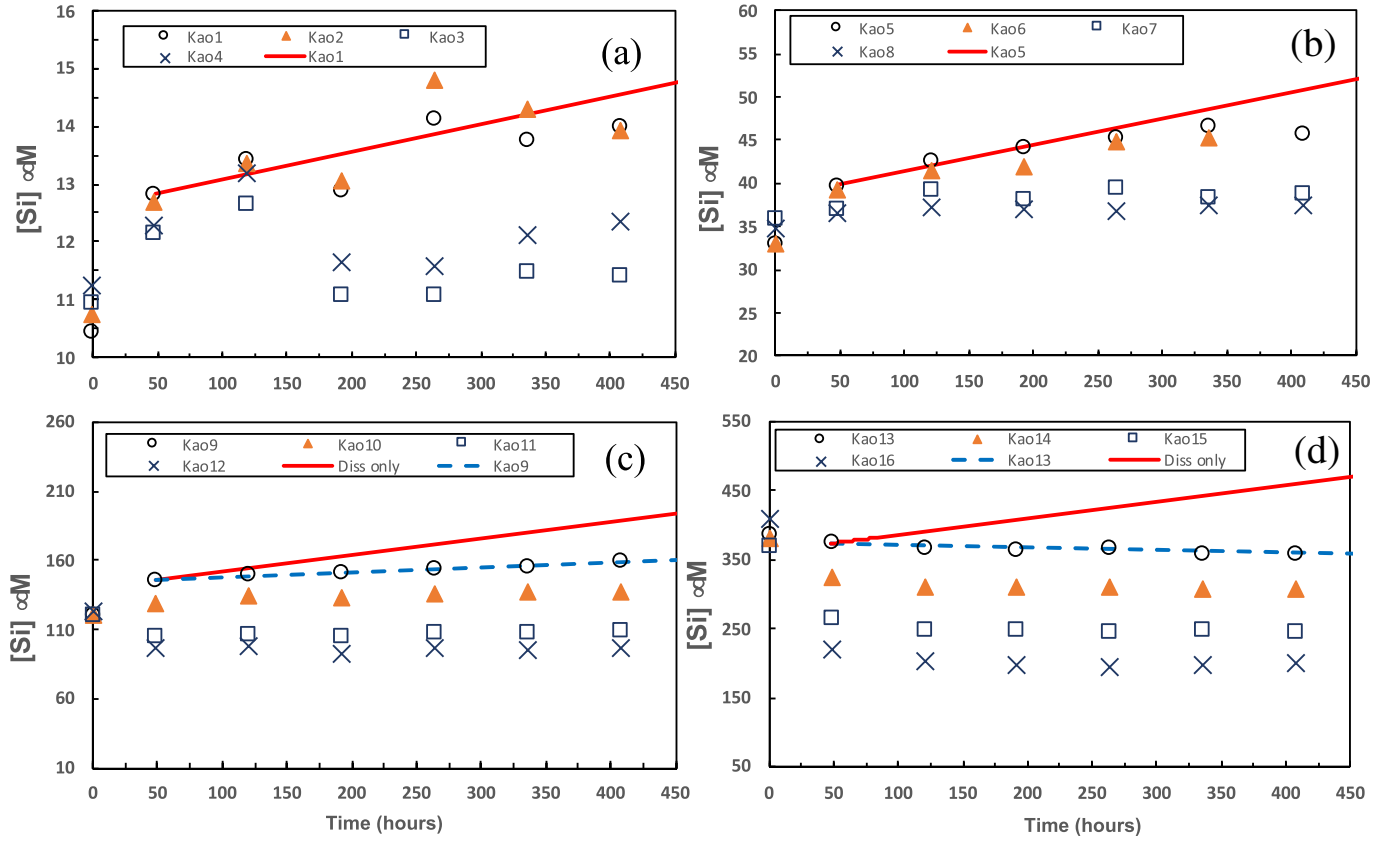

Fig. 2. Temporal evolution of Si concentrations. Symbols represent experimental data. Si analytical uncertainties were < ± 5%. The red solid lines denote ($[Si]^o + \Delta[Si]_{kaol}$) values; and blue dashed lines were fitted to the experimental [Si] with Si precipitation rates. The difference between the two lines represents Si precipitated from the solution. For the clarity, only one line is shown for each group. (a) and (b): No SI precipitation in Kao1 and Kao5. (c): A significant amount of Si was precipitated in Kao9; (d): Net Si precipitation was observed. Note the high [Si] in this group of experiments. (For interpretation of the references to colour in this figure legend, the reader is referred to the web version of this article.)

In all experiments, Al precipitation occurred, even in experiments that did not show Si precipitation. In general, Al concentrations were not systematic when plotted against either time or pH. The Al precipitation rates were similarly estimated as for Si. They are listed in Table 2. The rate of Al precipitation exceeded Si rates in all but Kao13–16 for which the initial [Si] was high (Fig. 2d).

4. Discussions

4.1. Precipitation of secondary phases and "did kaolinite precipitate?"

The experimental data show clearly the precipitation of Al and Si in these near-neutral pH solutions. The precipitates were probably amorphous or poorly crystalline secondary phases that were supersaturated such as allophane, imogolite, and gibbsite. The precipitation process is likely a path-dependent kinetic process and therefore may differ in each batch, which explains the scatter and conflicts in near-equilibrium and near-neutral pH experimental data. In contrast, the Si isotope ratio method gave consistent kaolinite dissolution rates in the presence of secondary phase precipitation.

To identify which phases precipitated in these experiments is extremely challenging. The Si:Al stoichiometric ratios are not consistent from experiment to experiment. It is likely that more than one secondary phase precipitated. The question of whether the reverse reaction of kaolinite precipitation has occurred in these kaolinite-supersaturated solutions is an important one, but that one probably could not be answered at this time. Yang and Steefel (2008) used synchrotron X-ray diffraction analysis for their kaolinite samples for which solution chemistry indicated possible kaolinite precipitation after reacting over the course of two months, but the results were not conclusive. Our experiments were at the same temperature (22 °C) but shorter than those of Yang and Steefel (2008).

4.2. Comparison with rate values in the literature

Comparing the kaolinite dissolution rates in this study to those in the literature merits caution. Rates from the isotope tracer method (this study) are unidirectional rates and cannot be compared to the near-equilibrium *net dissolution rates* determined with the conventional method (Devidal et al., 1997; Nagy et al., 1991; Nagy and Lasaga, 1993; Yang and Steefel, 2008).

Theoretically, the rates in this study are comparable to those of *far-from-equilibrium rates* if the reaction mechanisms are the same at far-from-equilibrium and near-equilibrium. A large number of far-from-equilibrium kaolinite dissolution experiments were conducted from 1964 to 2008 (Bauer and Berger, 1998; Bauer et al., 1998; Cama et al., 2002; Carroll and Walther, 1990; Devidal et al., 1997; Ganor et al., 1995; Huertas et al., 1999; Metz and Ganor, 2001; Nagy et al., 1991; Nagy and Lasaga, 1993; Polzer and Hem, 1965; Wieland and Stumm, 1992; Yang and Steefel, 2008). These experiments have been reviewed and the rates fitted as a function of pH (Brantley, 2008; Declercq and Oelkers, 2014; Marini, 2006; Marty et al., 2015; Nagy, 1995; Palandri and Kharaka, 2004; Schott et al., 2009). Fig. 3 shows the comparison for rates measured at ~25 °C. Rates in this study agree with those from Carroll and Walther (1990) but were more than an order of magnitude higher than those from Huertas et al. (1999) at the same pH. Note the scatter and conflict of rates for the far-from-equilibrium rate values in the figure, which probably also resulted from secondary phase

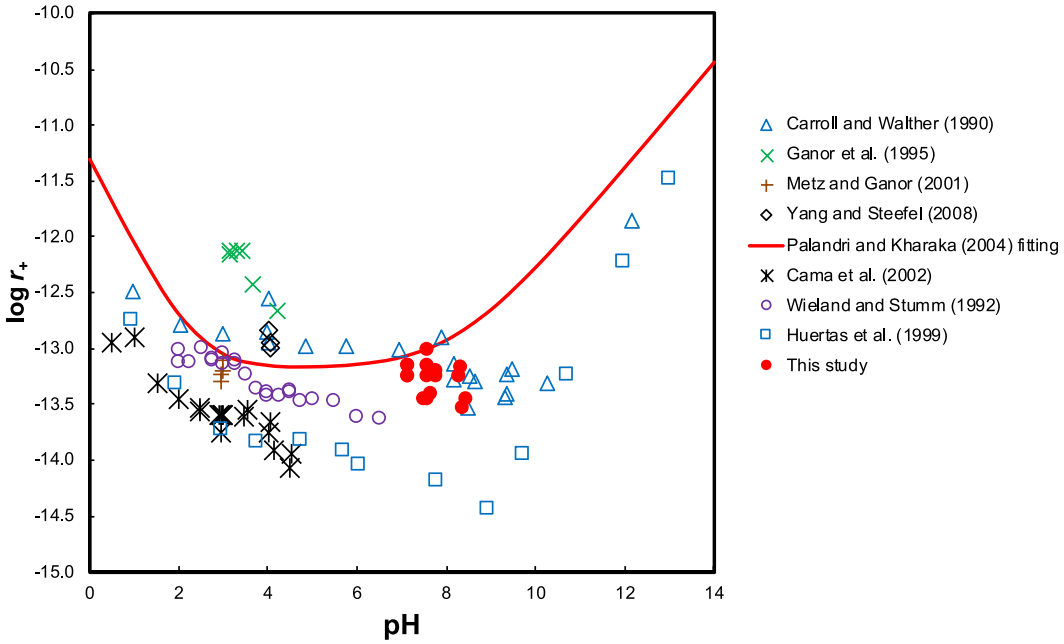

Fig. 3. Experimentally measured kaolinite dissolution rates at ~25 °C and various pH from the literature. The red solid line is the recommendation by Palandri and Kharaka (2004). (For interpretation of the references to colour in this figure legend, the reader is referred to the web version of this article.)

precipitation. As kaolinite solubility is low and Al and Si tend to precipitate at near-neutral pH, conventional experiment methods that uses [Si] or [Al] are problematic. Our rates are comparable to those of Yang and Steefel (2008) when the pH effect is taken into account.

4.3. Kaolinite dissolution in supersaturated solutions

Also theoretically, kaolinite dissolution should continue in solutions that are supersaturated with respect to kaolinite even though the net reaction is Si precipitation (and kaolinite precipitates in kaolinite-undersaturated solutions near-equilibrium). Chemical equilibrium is dynamic (Van't Hoff, 1884). With Si isotopes, we were able to observe kaolinite dissolution in supersaturated solutions experimentally.

The statement about kaolinite supersaturation needs to be qualified because kaolinite solubility is controversial and recommended solubility product (K_{sp}) values span over two orders of magnitude in the literature (Tutolo et al., 2014). However, the experiments in this study covered such a wide range of saturation levels that there is little doubt that some of our experiments were in kaolinite-supersaturated solutions. Fig. 4 shows a phase diagram in which the kaolinite solubility boundary was constructed using the standard state Gibbs free energy of formation ($\Delta_f G^o$) for kaolinite from Holland and Powell (2011) and log K values of Al and Si aqueous species recommended by Tagirov and Schott (2001) and Rimstidt (1997), respectively. This is the set of thermodynamic properties compiled in SUPCRTBL (Zimmer et al., 2016). The kaolinite solubility calculated from SUPCRTBL is similar to that recommended by Tutolo et al. (2014). According to these thermodynamic properties (thick black line in Fig. 4), all experiments were supersaturated with respect to kaolinite.

However, if the K_{sp} value recommended by Yang and Steefel (2008) or Helgeson et al. (1978) is used instead (dashed line in Fig. 4), still half of our experiments were supersaturated. This is because the saturation states in our experiments covered a wide range. In terms of saturation indices (SI), it spans seven units (e.g., 0.94 to 7.87). In terms of the Gibbs free energy of reaction $\Delta_r G$, the span was 17.17 kJ mol^{-1}. The argument about kaolinite solubility products is over about two log units (Tutolo et al., 2014). For example, the difference between log Ks from SUPCRTBL and Yang and Steefel (2008) is 2.2.

5. Conclusions

Conventionally, experiments to determine clay mineral dissolution and precipitation rates have used Si and Al concentrations. However, this method is problematic when applied to near-neutral pH solutions at ambient temperatures because the solubility of clay minerals is low and Si, and particularly Al, tends to precipitate as secondary phases. As a result, no kaolinite dissolution rate data at near-neutral pH and near-equilibrium had yet been determined. However, the vast majority of natural waters are near-neutral pH and are supersaturated with respect to kaolinite and other clays (Drever, 1988; Langmuir, 1997). This study measured kaolinite dissolution rates at 22 °C, pH 7.1–8.5, and near-equilibrium (kaolinite supersaturated) conditions. Our rates are therefore applicable to the studies of natural waters.

The dissolution rate derived from ^{29}Si isotope tracer is also a different kind of kinetic data from those reported in the literature. The rates are *unidirectional* (dissolution only); unlike net rates (dissolution minus precipitation) as in the literature. Applications of these experimental rates do not require extrapolation from far-from-equilibrium to near-equilibrium conditions (e.g., Huertas et al., 1999 and others in Fig. 3), which would require a number of assumptions that are difficult to validate (e.g., the same reaction mechanisms; the Principle of Detailed Balance applies to the overall reactions).

Finally, the consistency of the Si isotope data in a grid of pH, [Si], and solid:solution ratios demonstrates the power of the isotope ratio method. Si and Al concentrations were collected for all experiments in this study. They are often inconsistent and non-systematic. We suspect that much of the scatter and conflicts in rate data at near-equilibrium and near-neutral pH conditions resulted from secondary phase precipitation. With the demonstration that the large changes of ^{29}Si/^{28}Si ratios in these spiked experimental systems can be inexpensively measured with ICP-MS, instead of multiple collector ICP-MS, Si isotope tracer experiments for clay minerals can be inexpensively conducted with a short turnaround time. It appears that this should be the experimental method of choice for future studies.

Data availability

Experimental data are provided with the journal as Supplementary

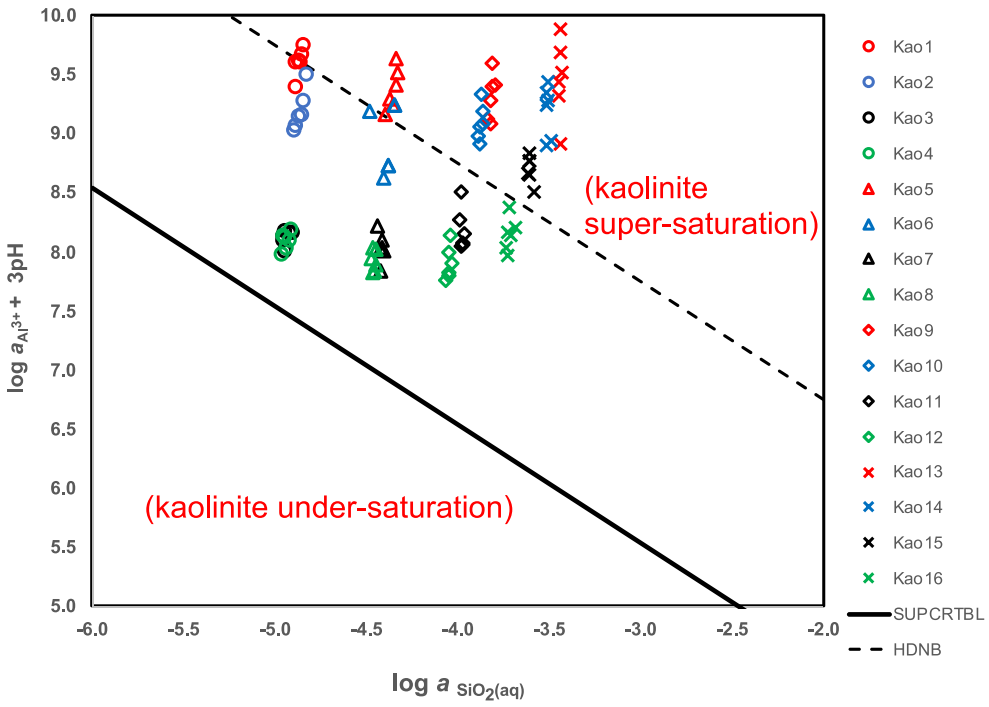

Fig. 4. Activity-activity phase diagram showing calculated equilibrium lines for kaolinite at 1 bar and 25 °C. The solid line was calculated using SUPCRTBL and is similar to the recommendation of Tutolo et al. (2014). The dashed line was calculated with K_{sp} recommended by Yang and Steefel (2008) and Helgeson et al. (1978). The experimental data of May et al., 1986) are located between these two lines (not shown). The two vertical lines are quartz and amorphous silica equilibrium, respectively. Symbols denote experimental data. Activities of Al^{3+} and $SiO_2^0(aq)$ were calculated from speciation modeling of experimental solutions.

Materials and at IUScholarWorks at doi.org/10.5967/qxym-q251.

Funding

This work was partially supported by the U.S. NSF grant EAR-19267343 and the Vice Provost for Research office through the program of Faculty Research Support Program at Indiana University.

Declaration of Competing Interest

None.

Acknowledgment

This work was partially supported by the U.S. NSF grant EAR-19267343 and the Vice Provost for Research office through the program of Faculty Research Support Program at Indiana University. We are grateful to Anne Hereford and Sara Loy for editing and to Ben Underwood for assistance with ICP-MS analyses and Ping Chen for lab assistance. Most of all, we wish to dedicate this work to Don Rimstidt, a beloved collaborator and friend who passed away prematurely. Don designed the experimental grid but did not live to see the experimental results. Comments from the Associate Editor Juraj Bujdak and two anonymous reviewers have helped improve the clarity of the manuscript.

Appendix A. Supplementary data

Supplementary data to this article can be found online at https://doi.org/10.1016/j.clay.2019.105284.

References

Bauer, A., Berger, G., 1998. Kaolinite and smectite dissolution rate in high molar KOH solutions at 35 degrees and 80 degrees C. Appl. Geochem. 13, 905–916.

Bauer, A., Velde, B., Berger, G., 1998. Kaolinite transformation in high molar KOH solutions. Appl. Geochem. 13, 619–629.

Brantley, S.L., 2008. Kinetics of mineral dissolution. In: Brantley, S.L., Kubicki, J.D., White, A.F. (Eds.), Kinetics of Water-Rock Interaction. Springer, New York, pp. 151–210.

Cama, J., Metz, V., Ganor, J., 2002. The effect of pH and temperature on kaolinite dissolution rate under acidic conditions. Geochim. Cosmochim. Acta 66, 3913–3926.

Carroll, S.A., Walther, J.V., 1990. Kaolinite dissolution at 25 °C, 60 °C, and 80 °C. Am. J. Sci. 290, 797–810.

Declercq, J., Oelkers, E.H., 2014. CarbFix Report: PHREEQC Mineral Dissolution Kinetics Database. https://www.or.is/sites/or.is/files/kinetic_database.pdf as of June 9, 2019. pp. 197.

Devidal, J.-L., Schott, J., Dandurand, J.-L., 1997. An experimental study of kaolinite dissolution and precipitation kinetics as a function of chemical affinity and solution composition at 150°C, 40 bars, and pH 2, 6.8, and 7.8. Geochim. Cosmochim. Acta 61, 5165–5186.

Drever, J.I., 1988. The Geochemistry of Natural Waters: Surface and Groundwater Environment. Prentice-Hall, Englewood Cliffs, New Jersey.

Ganor, J., Mogollon, J.L., Lasaga, A.C., 1995. The effect of pH on kaolinite dissolution rates and on activation energy. Geochim. Cosmochim. Acta 59, 1037–1052.

Gruber, C., Harpaz, L., Zhu, C., Bullen, T.D., Ganor, J., 2013. A new approach for measuring dissolution rates of silicate minerals by using silicon isotopes. Geochim. Cosmochim. Acta 104, 261–280.

Helgeson, H.C., Delany, J.M., Nesbitt, H.W., Bird, D.K., 1978. Summary and critique of the thermodynamic properties of rock forming minerals. Am. J. Sci. 569–592 278A.

Holland, T., Powell, R., 2011. An improved and extended internally consistent thermodynamic dataset for phases of petrological interest, involving a new equation of state for solids. J. Metamorph. Geol. 29, 333–383.

Huertas, F.J., Chou, L., Wollast, R., 1999. Mechanism of kaolinite dissolution at room temperature and pressure Part II: kinetic study. Geochim. Cosmochim. Acta 63, 3261–3275.

Langmuir, D., 1997. Aqueous Environmental Geochemistry. In: Prentice Hall. Upper Saddle River, New Jersey.

Liu, Z., Rimstidt, J.D., Zhang, Y., Zhu, C., 2016. A stable isotope doping method to test the range of applicability of detailed balance. Geochem Perspect Lett 2, 78–86.

Madsen, F.T., 1998. Clay mineralogical investigations related to nuclear waste disposal. Clay Miner. 33, 109–129.

Marini, L., 2006. Geological Sequestration of Carbon Dioxide: Thermodynamics, Kinetics, And Reaction Path Modeling. Elsevier.

Marty, N.C., Claret, F., Lassin, A., Tremosa, J., Blanc, P., Madé, B., Giffaut, E., Cochepin, B., Tournassat, C., 2015. A database of dissolution and precipitation rates for clay-rocks minerals. Appl. Geochem. 55, 108–118.

May, H.M., Klnniburgh, D.G., Helmke, P.A., Jackson, M.L., 1986. Aqueous dissolution, solubilities and thermodynamic stabilities of common aluminosilicate clay minerals: kaolinite and smectites. Geochim. Cosmochim. Acta 50, 1667–1677.

McBride, M.B., 1994. Environmental Chemistry of Soils. Oxford University Press, New York.

Metz, V., Ganor, J., 2001. Stirring effect on kaolinite dissolution rate. Geochim. Cosmochim. Acta 65, 3475–3490.

Murray, M., 1999. Applied clay mineralogy today and tomorrow. Clay Clay Miner. 34, 39–49.

Nagy, K.L., 1995. Dissolution and precipitation kinetics of sheet silicates. In: White, A.F., Brantley, S.L. (Eds.), Chemical Weathering Rates of Silicate Minerals. Mineralogical Society of America, pp. 173–225.

Nagy, K.L., Lasaga, A.C., 1993. Kinetics of simultaneous kaolinite and gibbsite precipitation. Geochim. Cosmochim. Acta 57, 4329–4337.

Nagy, K.L., Blum, A.E., Lasaga, A.C., 1991. Dissolution and precipitation kinetics of kaolinite at 80° C and pH 3: the effect of deviation from equilibrium. Am. J. Sci. 291, 649–686.
Opfergelt, S., Delmelle, P., 2012. Silicon isotopes and continental weathering processes: assessing controls on Si transfer to the ocean. Compt. Rendus Geosci. 344, 723–738.
Palandri, J.L., Kharaka, Y.K., 2004. A Compilation Of Rate Parameters Of Water-Mineral Interaction Kinetics For Application To Geochemical Modeling. US Geological Survey Open File Report 2004–1068.
Parkhurst, D.L., Appelo, C., 2013. Description of input and examples for PHREEQC version 3—a computer program for speciation, batch-reaction, one-dimensional transport, and inverse geochemical calculations. In: US geological survey techniques and methods, book 6, pp. 497.
Polzer, W.L., Hem, J.D., 1965. Dissolution of kaolinite. J. Geophys. Res. 70, 6233.
Rimstidt, J.D., 1997. Quartz solubility at low temperatures. Geochim. Cosmochim. Acta 61, 2553–2558.
Rimstidt, J.D., 2014. Geochemical Rate Models: An Introduction to Geochemical Kinetics. Cambridge University Press.
Schott, J., Pokrovsky, O., Oelkers, E.H., 2009. The link between mineral dissolution/precipitation kinetics and solution chemistry. In: Oelkers, E.H., Schott, J. (Eds.), Reviews in Mineralogy and Geochemistry. MSA, pp. 207–258.
Stefansson, A., 2001. Dissolution of primary minerals of basalt in natural waters: I. Calculation of mineral solubilities from 0 C to 350 C. Chem. Geol. 172, 225–250.
Su, C., Harsh, J.B., 1994. Gibbs free energies of formation at 298 K for imogolite and gibbsite from solubility measurements. Geochim. Cosmochim. Acta 58, 1667–1677.
Su, C.M., Harsh, J.B., 1998. Dissolution of allophane as a thermodynamically unstable solid in the presence of boehmite at elevated temperatures and equilibrium vapor pressures. Soil Sci. 163, 299–312.
Tagirov, B., Schott, J., 2001. Aluminum speciation in crustal fluids revisited. Geochim. Cosmochim. Acta 65, 3965–3992.
Thompson, H.A., 1998. Dynamic Ion Partitioning Among Dissolved, Adsorbed, And Precipitated Phases In Aging Cobalt(Ii)/Kaolinite/Water Systems. Doctoral dissertation. Stanford University, pp. 540.
Thompson, H.A., Parks, G.A., Brown, G.E., 1999. Dynamic interactions of dissolution, surface adsorption, and precipitation in an aging cobalt(II)-clay-water system. Geochim. Cosmochim. Acta 63, 1767–1779.
Tutolo, B.M., Kong, X.-Z., Seyfried Jr., W.E., Saar, M.O., 2014. Internal consistency in aqueous geochemical data revisited: applications to the aluminum system. Geochim. Cosmochim. Acta 133, 216–234.
Van't Hoff, J.H., 1884. Etudes De Dynamique Chimique. Frederic Muller & Co.
Wieland, E., Stumm, W., 1992. Dissolution kinetics of kaolinite in acidic aqueous solutions at 25 °C. Geochim. Cosmochim. Acta 56, 3339–3355.
Yang, L., Steefel, C.I., 2008. Kaolinite dissolution and precipitation kinetics at 22° C and pH 4. Geochim. Cosmochim. Acta 72, 99–116.
Zhu, C., Liu, Z., Zhang, Y., Wang, C., Schearer, A., Zhang, G., Georg, R.B., Yuan, H.-l., Rimstidt, J.D., 2016. Measuring silicate dissolution rates using Si isotope doping. Chem. Geol. 445, 146–163.
Zimmer, K., Zhang, Y., Lu, P., Chen, Y., Zhang, G., Dalkilic, M., Zhu, C., 2016. SUPCRTBL: A revised and extended thermodynamic dataset and software package of SUPCRT92. Comput. Geosci. 90, 97–111 Part A.